Dielectric response to the low-temperature magnetic defect structure and spin state transition in polycrystalline $LaCoO_3$

Rainer Schmidt,[1,*] J. Wu,[2] C. Leighton,[2] and I. Terry[3]
[1]*Engineering Materials, The University of Sheffield, Mappin Street, Sheffield S1 3JD, United Kingdom*
[2]*Department of Chemical Engineering and Materials Science, University of Minnesota, Minneapolis, Minnesota 55455, USA*
[3]*Department of Physics, University of Durham, South Road, Durham DH1 3LE, United Kingdom*
(Received 11 November 2008; revised manuscript received 28 January 2009; published 6 March 2009)

The dielectric and magnetic properties and their correlations were investigated in polycrystalline perovskite $LaCoO_{3-\delta}$. The intrinsic bulk and grain-boundary (GB) dielectric relaxation processes were deconvoluted using impedance spectroscopy between 20 and 120 K, and resistivity and capacitance were analyzed separately. A thermally induced magnetic transition from a Co^{3+} low-spin (LS) ($S=0;t_{2g}^6e_g^0$) to a higher spin state occurs at $T_{s1}\approx 80$ K, which is controversial in nature and has been suggested to be an intermediate-spin (IS) state ($S=1;t_{2g}^5e_g^1$) or a high-spin (HS) state ($S=2;t_{2g}^4e_g^2$) transition. This spin state transition was confirmed by magnetic-susceptibility measurements and was reflected in the impedance by a split of the single GB relaxation process into two coexisting contributions. This apparent electronic phase coexistence at $T>80$ K was interpreted as a reflection of the coexistence of magnetic LS and IS/HS states. At lower temperatures ($T\leq 40$ K) perceptible variation in bulk dielectric permittivity with temperature appeared to be correlated with the magnetic susceptibility associated with a magnetic defect structure. At 40 K$<T<T_{s1}$, separated GB and bulk resistivity vs T curves were consistent with localized polaron Mott variable-range hopping (VRH) based on impurity conduction. Below 40 K, a crossover from impurity Mott's VRH to another type of thermally activated charge transport was detected, which was correlated with the appearance of the defect-related magnetism.

DOI: 10.1103/PhysRevB.79.125105 PACS number(s): 72.80.Ga, 75.30.Kz, 77.22.Ch

I. INTRODUCTION

The perovskite compound $LaCoO_3$ (LCO) has attracted considerable interest in the past due to a thermally induced spin state transition from a nonmagnetic low-spin (LS) state ($S=0$) to a paramagnetic intermediate-spin (IS) state ($S=1$) or high-spin (HS) state ($S=2$) at T_{s1} of 70–90 K.[1–5] In most studies the crystal symmetry of perovskite LCO is referred to as the trigonal space group $R\bar{3}c$, no.167, although a small monoclinic distortion due to orbital ordering has also been reported.[6] The electronic configuration of the Co^{3+} cations on the octahedral perovskite B sites is $t_{2g}^6e_g^0$ in the $S=0$ ground state.[7] The crystal-field energy splitting of the octahedral Co d-electron energy levels into t_{2g} and e_g levels is only marginally larger than Hund's coupling energy (Fig. 1). This small energy difference can be overcome by thermal activation, and a Co^{3+} t_{2g} electron can transfer into the e_g level. The compound was suggested to adopt the IS state ($S=1;t_{2g}^5e_g^1$) above 70–90 K,[8–10] although an alternative Co^{3+} HS state transition instead has been suggested as well ($S=2;t_{2g}^4e_g^2$).[11–16] The number of publications in the literature favoring one or the other model are split approximately even, and the nature of the LCO spin state transition is still a matter of debate to date.[17] Transitional features in the magnetic susceptibility and an insulating-to-metallic charge transport transition by heating across $T_{s2}\approx 500$ K have been reported. In the model favoring the LS-IS state transition at ≈80 K, T_{s2} was interpreted as an IS-to-HS state transition (see Fig. 1).[18–20] Alternatively, in the LS-HS state transition model, the compound is assumed to be in an inhomogeneous mixed state of LS and HS areas at $T_{s2}>T>T_{s1}$,[21,22] and it transforms to a metallic IS state at $T>T_{s2}$.[23] In the latter model, the mixing ratio or population levels of LS and HS states would be temperature dependent and magnetic phase coexistence of LS and HS states is implied at $T_{s2}>T>T_{s1}$. Another mixed LS-IS-HS state model[24] claims that LS and IS states are both populated above T_{s1}, and the HS state starts to be populated gradually above ≈250 K. This would imply phase coexistence of LS and IS states at 250 K$>T>T_{s1}$ and phase coexistence of all three spin states LS, IS, and HS at $T>250$ K.

LCO exhibits paramagnetic behavior in the IS/HS states at $T>T_{s1}$, whereas the LS state at $T<T_{s1}$ is believed to be diamagnetic.[25] In reality, the low-temperature magnetization in LCO shows a sharp upturn at ≈40 K upon cooling in a paramagnetic "Curie tail" fashion. A magnetic phase transition is not evident from structural neutron or x-ray diffraction data, and this magnetic structure is believed to arise

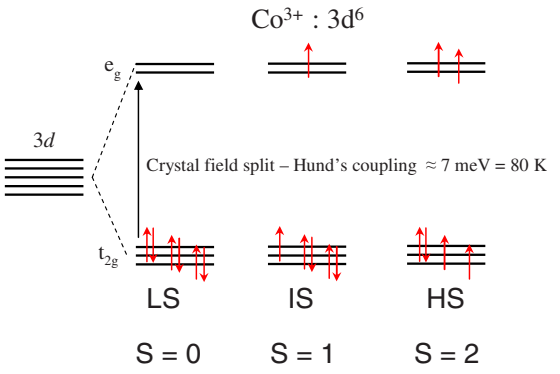

FIG. 1. (Color online) Electron energy levels of the LS, IS, and HS states in $LaCoO_{3-\delta}$ with $3d^6$ Co^{3+} electron configuration.

from magnetic defects induced by oxygen vacancies. Such oxygen vacancies have been shown to exist at all temperatures from refined neutron-diffraction data.[26] The nature of such a magnetic defect structure is still not fully understood. It has been proposed that localized electrons, possibly bound to oxygen vacancies, induce magnetic moments to their local magnetic environment. This may be regarded as the formation of magnetic polarons[5] or excitons.[27,28] Similarly, magnetic clusters or spin state polarons have been observed in lightly hole-doped $La_{1-x}Sr_xCoO_3$, $x=0.002$,[29] and were interpreted as a precursor to the fully developed ferromagnetic phase at higher x. Alternatively, a ferromagnetic surface effect has been claimed to be responsible,[30] but the magnetic defect and polaron model is more established now. Furthermore, Co^{2+} magnetic cations may be present in LCO to partially compensate for oxygen vacancies. This may lead to another magnetic impurity, i.e., Co^{2+} $(S=\frac{1}{2};t_{2g}^6e_g^1)$ in the intrinsically diamagnetic Co^{3+} LS ground state.

The electrical properties of both single-crystal and polycrystalline materials have been investigated by a number of authors. Thermopower measurements have demonstrated that hole conduction dominates the electrical transport at temperatures above ≈ 75 K,[7,31] which is in agreement with Hall measurements at higher temperatures.[32] The direct current (dc) charge transport properties in polycrystalline LCO have previously been measured at $T \geq 50$ K,[33] and it was suggested that impurity-localized electron hopping is active at low temperatures. The magnetoresistance is positive and anisotropic below 60 K, but it changes to negative values and is isotropic at higher temperatures. A peak in magnetoresistance has been reported to occur at T_{s1} as a reflection of the spin state transition.[33]

In the present work, alternating current (ac) impedance spectroscopy was used to show that the macroscopic charge transport and dielectric properties are both inhomogeneous in polycrystals due to the ceramic microstructure. Grain-boundary (GB) and intrinsic bulk relaxation processes were deconvoluted and analyzed separately.

Correlations of the dielectric and magnetic structure of $LaCoO_{3-\delta}$ were investigated at low temperatures in the Curie tail regime and across the spin state transition at T_{s1}. Such correlations, often termed magnetoelectric (ME) coupling, have attracted considerable interest recently[34] and have been shown to be strongest across magnetic or electronic phase transitions.[35] Interest in ME coupling effects is driven by the prospect to develop materials with strongly coupled dielectric and magnetic properties. However, dielectric-magnetic correlations in oxides have not been investigated so far across a spin state transition and in the presence of a magnetic defect structure, which has motivated the study presented here.

II. EXPERIMENT

$LaCoO_{3-\delta}$ powder was synthesized from La_2O_3 and Co_3O_4 starting materials by the standard solid-state reaction method. The starting materials were thoroughly ground, reacted in air for 7 days at 980 °C, and cooled over a period of 6 h to room temperature. Pellets of the calcinated powder were then cold pressed under 8000 psi and were sintered in air for 1 day at 1200 °C and then slow cooled over a period of 24 h. Structural and compositional characterizations of the pellets are described elsewhere.[36]

Electrodes were deposited onto a pellet by covering both sides with Ag paste and metallization was achieved by firing at 800 °C for 2 h. Only small deviations in the oxygen stoichiometry are expected due to this firing process. The value of $\delta=0.02\pm0.02$ was obtained from iodometric titration measurements of the as-synthesized $LaCoO_{3-\delta}$ pellet, suggesting that the sample may be close to the nominal stoichiometry. Impedance spectroscopy was carried out at 20–120 K using an Edwards Cryodrive 1.5 closed cycle cryocooler, an Oxford Instruments sample chamber, an ITC 5035 Oxford Instruments temperature controller, and an Agilent E4980A Precision LCR meter. Real (Z') and imaginary (Z'') parts of the complex impedance (Z^*) were obtained separately and were transformed into the complex capacitance (C^*) and modulus (M^*) notations using the standard transformations.[37] Impedance and capacitance values were normalized by the pellet geometry and expressed as specific parameters z', z'', c', and c''. The electrodes of the pellet were removed and magnetic-susceptibility measurements were carried out under field-cooled and zero-field-cooled conditions at a magnetic field of 10 kOe using a Quantum Design MPMS (magnetic properties measurement system XL) superconducting quantum interference device magnetometer, in the temperature range of 2–330 K.

III. IMPEDANCE SPECTROSCOPY

ac impedance spectroscopy experiments consist effectively of a time (t)-dependent alternating voltage signal U of angular frequency ω and amplitude U_0, i.e., $U(\omega,t)=U_0\cos(\omega t)$, applied to a sample, and the phase shift γ and amplitude I_0 of the current response signal I are determined, $I(\omega,t)=I_0\cos(\omega t-\gamma)$. The current response of ideal circuit elements is (1) in phase with the applied voltage in case of a resistor R, (2) out of phase by $\gamma=-\pi/2$ for a capacitor C, and (3) out of phase by $\gamma=+\pi/2$ for an inductor. All phase angles are time independent for a given frequency, which allows defining the impedance as a time-independent complex number Z^*. The impedance fraction in phase with $U(\omega,t)$ is defined as the real, and the $\pm\pi/2$ out of phase part is defined as the positive/negative imaginary part, i.e., $Z^*=Z'+iZ''$.[37,38] Impedance spectra of separated real and imaginary parts are commonly obtained over a large frequency range (typically $f\sim 10$ Hz–1 MHz). The complex impedance of electrode-sample interface, GB, and bulk relaxation processes in polycrystalline materials can each be described and modeled by an RC element consisting of a resistor and capacitor in parallel, and the macroscopic impedance is just the sum of the individual series RC impedances. The magnitude of each specific capacitance $c(=\varepsilon_0\varepsilon_r)$ allows the originating effect of the relaxation to be identified (electrodes, GB, or bulk),[39] and the different components of the macroscopic dielectric properties can be deconvoluted.[40] ε_r is the real part of the effective dielectric permittivity of the respective capacitor and ε_0 for vacuum.

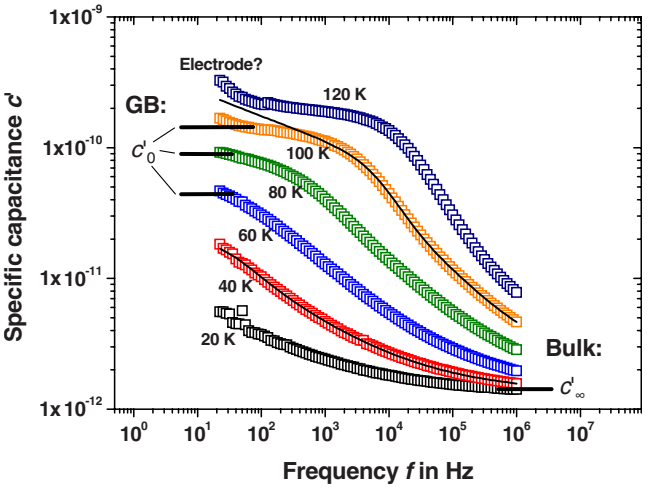

FIG. 2. (Color online) Real part of the specific capacitance c' vs frequency f; the low-frequency plateau corresponds to the GB relaxation; the high-frequency plateau represents the intrinsic bulk contribution. Small indications for an electrode interface effect are displayed at the low-frequency end at 100 and 120 K by a slight upturn of the capacitance. The solid lines represent fits to the data at 40 and 100 K using model 1.

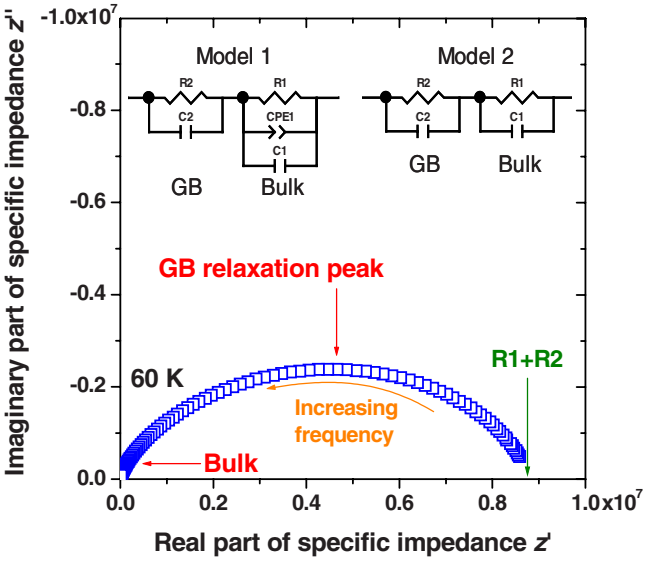

FIG. 3. (Color online) Complex specific impedance plots of z'' vs z'; the GB and bulk relaxation processes cannot be resolved due to strong overlap. Equivalent circuit models describing intrinsic bulk ($R1$-CPE1-$C1$)/($R1$-$C1$) and grain-boundary ($R2$-$C2$) contributions.

The impedance data collected from $LaCoO_{3-\delta}$ polycrystals at various temperatures are presented in Fig. 2 as the real part of the complex specific capacitance (c') plotted vs frequency (f) on a double-logarithmic scale. Two distinct c' capacitance plateaus (c'_0 and c'_∞) can be seen clearly at $T \geq 60$ K, which suggests an inhomogeneous electronic structure due to two different relaxation processes. At the specific temperature and frequency ranges displayed, the two relaxations may well reflect the intrinsic bulk and a GB contribution. Each relaxation was modeled by an RC element, and two RC elements in series can then account for the two relaxation processes. Two series RC elements give rise to two approximately frequency-independent c' plateaus (c'_0 and c'_∞) in c' vs f plots (Fig. 2) and give rise to two semicircles on a complex impedance plot of negative imaginary ($-z''$) vs real parts (z') of the specific impedance.[38,39] RC elements can be characterized by their relaxation times $\tau(\tau = RC = \rho\varepsilon_0\varepsilon_r)$, where R and ρ are the resistance and resistivity and C is the capacitance. Note that τ is independent of sample geometry. The small upturn of c' at the low-frequency end at $T \geq 100$ K may indicate the onset of an electrode-sample interface relaxation.

The complex impedance plot at 60 K (Fig. 3) displays only one strongly suppressed semicircle, which can be associated with a strong overlap of two semicircles due to similar time constants τ of the two relaxation processes. The complex impedance plots may be inappropriate in this instance to demonstrate the electronic heterogeneity of the sample. However, the bulk and GB relaxations can be distinguished and deconvoluted unambiguously on plots of $-z''$ vs f and the modulus plot M'' vs f (Fig. 4), where the GB and bulk relaxation peaks are displayed separately at clearly different frequencies. For ideal dielectric relaxations described by ideal RC elements the relaxation peaks adopt the shape of a Lorentz function. Figure 4 shows that this may not be the case here and relaxation peak broadening is evident. In $LaCoO_{3-\delta}$, the GB and bulk relaxation peak broadening may be particularly pronounced. This can be directly correlated with a broad distribution of the relaxation times τ, which implies a broad distribution of the resistivity and/or the relative dielectric permittivity values across the sample.[37] One may consider the sample as being made up of an infinite number of infinitesimal small building blocks. The resistivity and relative dielectric permittivity values of each building block, plotted out on a statistical scale, may both show a distribution possibly in a Gaussian style fashion. The origin of such distributions can be of physical or chemical nature. Strong disorder of the electron potential, typical for ceramic

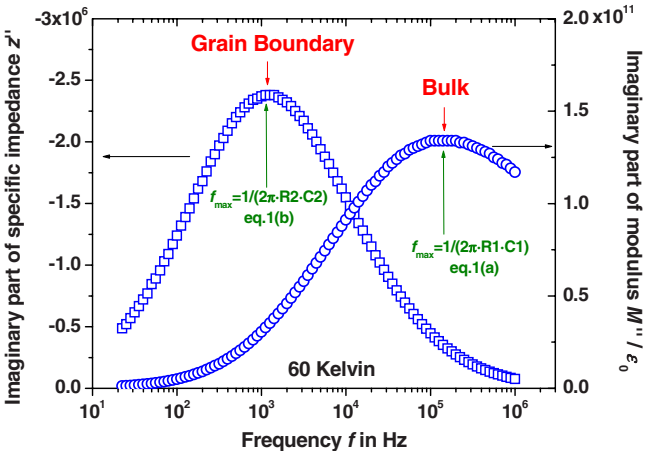

FIG. 4. (Color online) Imaginary parts of the specific impedance z'' and modulus function M'' vs frequency; the GB and bulk relaxations can be clearly resolved. Equation (1a) and (1b) allows determining the R and C values from f_{max} for the two RC elements representing the bulk ($R1$ and $C1$) and GB ($R2$ and $C2$) relaxations.

materials, or simply local variations in stoichiometry may both be plausible explanations.

Fits to the data were attempted using a common equivalent circuit model (model 1 in Fig. 3), where the nonideality (relaxation-time distribution) of the bulk relaxation process is accounted for by the use of an additional parallel constant-phase element (CPE1). However, clear deviations at low frequency can be seen in Fig. 2 for $T=100$ K. Therefore, $R1$, $R2$, and $C2$ values obtained from such fits may not be reliable. No alternative and physically meaningful equivalent circuit could be found to fit the data satisfactorily. Consequently, the nonideality of the relaxations was neglected and ideal behavior was assumed (model 2). The ideal circuit $R1$, $R2$, $C1$, and $C2$ values were determined from the spectroscopic plots as described in the following.

The relaxation peak frequencies $f_{\max}$ from z'' and M'' vs f plots (Fig. 4) were believed to be unaffected by the peak broadening (nonideality) and yielded two expressions [Eq. (1a) and Eq. (1b) in Fig. 4] containing $R1$ and $C1$ for the bulk (from M'' vs f) and $R2$ and $C2$ for the GB relaxation (from z'' vs f). The $f_{\max}$ values for ideal RC elements, where $-z''$ and M'' are at a maximum, are both given by the same general expression

$$f_{\max} = \frac{1}{2\pi RC} = \frac{1}{2\pi\rho\varepsilon_r}. \tag{1}$$

Equation (1) was applied to both RC elements [resulting in Eq. (1a) and (1b)] using model 2 in Fig. 3. In the case of $R1$-$C1$, Eq. (1) was applied to the M'' vs f plot, and for $R2$-$C2$ Eq. (1) was applied to the z'' vs f plots (see Fig. 4). Additionally, the high and low c' plateaus in c' vs f plots (Fig. 2), $c'_\infty = \lim_{f\to\infty} c'(f)$ and $c'_0 = \lim_{f\to 0} c'(f)$ for two ideal RC elements in series (GB and bulk), are given by

$$c'_\infty = \lim_{f\to\infty} c'(f) = \frac{C1\cdot C2}{(C1+C2)}, \tag{2a}$$

$$c'_0 = \lim_{f\to\infty} c'(f) = \frac{C1\cdot R1^2 + C2\cdot R2^2}{R1^2 + 2R1\cdot R2 + R2^2}. \tag{2b}$$

Using Eq. (1a) and (1b) and Eqs. (2a) and (2b), $R1$, $R2$, $C1$, and $C2$ were determined from experimental values for $f_{\max}$ in z'' vs f and M'' vs f, c'_∞ and c'_0. Constraints to the $R1$ and $R2$ values were applied in a way such that $(R1+R2)$ would correspond to the low-frequency z' axis (x axis) intercept z'_0 in the z'' vs z' plots (see Fig. 3),

$$z'_0 = \lim_{f\to 0} z'(f) = R1 + R2. \tag{3}$$

This analysis yielded a unique solution and was carried out at each temperature.

IV. RESULTS AND DISCUSSION

The bulk relative dielectric permittivity values obtained were plotted as a function of temperature in Figs. 5(a) and 5(b) together with the magnetization M and magnetic susceptibility χ. The magnetic data confirm the LS-to-IS transition at $T_{s1} \approx 70-90$ K. At low temperatures ($T \leq 40$ K) the

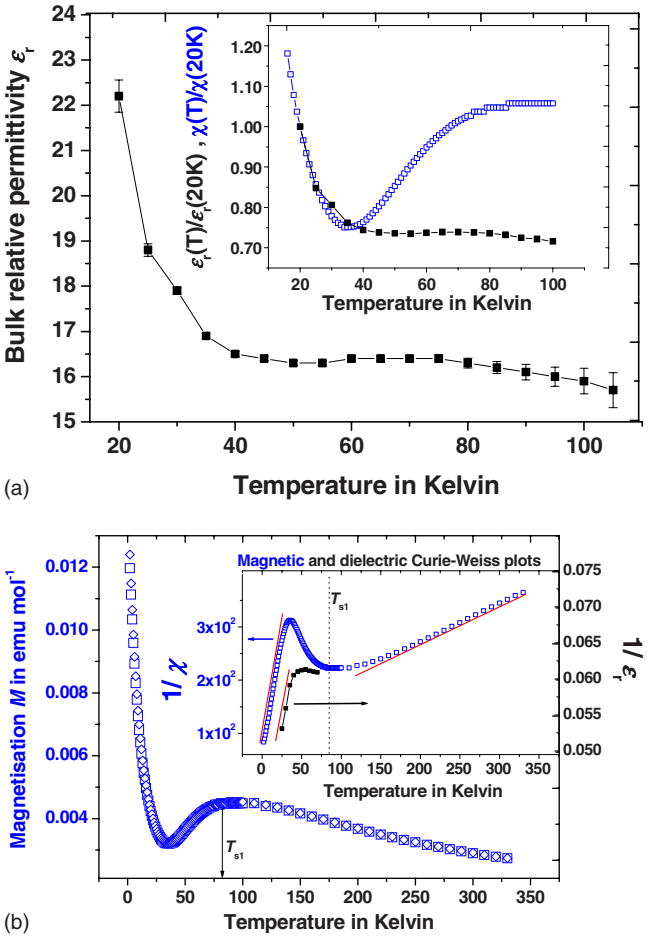

FIG. 5. (Color online) (a) Intrinsic bulk relative dielectric permittivity (■) as a function of temperature. Inset: normalized bulk permittivity (■) and normalized magnetic susceptibility (□) vs temperature; (b) field-cooled (◇) and zero-field-cooled (□) magnetizations measured as a function of temperature at a field of 10 kOe. Inset: bulk dielectric (■) and magnetic (□) Curie-Weiss plots. Red solid lines are guide to the eyes.

magnetization shows an upturn in a Curie tail fashion, which was associated with a magnetic defect structure originating from the formation of magnetic polarons (excitons). The shape of the bulk permittivity ε' vs T curve shows clear correlations to the magnetic susceptibility χ vs T below $T \leq 40$ K, where the magnetic Curie tail is active [Fig. 5(a) inset]. On the other hand, dielectric response to the magnetic spin-state transition T_{s1} appears to be weak in magnitude.

Previously, dielectric response related to magnetic polarons was observed in the dilute magnetic semiconductor $Cd_{1-x}Mn_xTe:In$,[41] where it was associated with a change in polarizability of electrons bound to In donors. The magnetization M vs T curve is displayed over the full temperature range in Fig. 5(b), where the magnetic defect structure ($T \leq 40$ K) as well as the regular paramagnetic phase at $T \geq T_{s1}$ both show approximate linearity in the magnetic Curie-Weiss plots [Fig. 5(b) inset]. By extrapolating both magnetic Curie-Weiss plots, the temperature axis (x axis) intercepts were found in both cases to be below 0 K, which can be associated with antiferromagnetic exchange interactions. The slope of the two magnetic Curie-Weiss plots varies

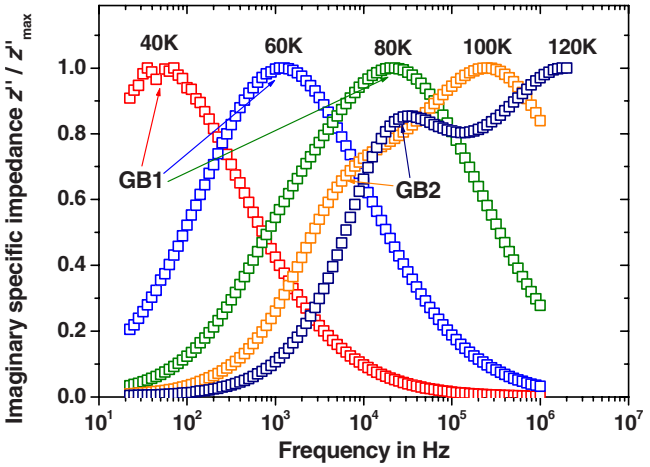

FIG. 6. (Color online) Imaginary part of impedance z'', normalized to z'' (f_{max}), vs frequency f. At the magnetic transition at ≈80 K the GB relaxation peak displayed splits into two contributions.

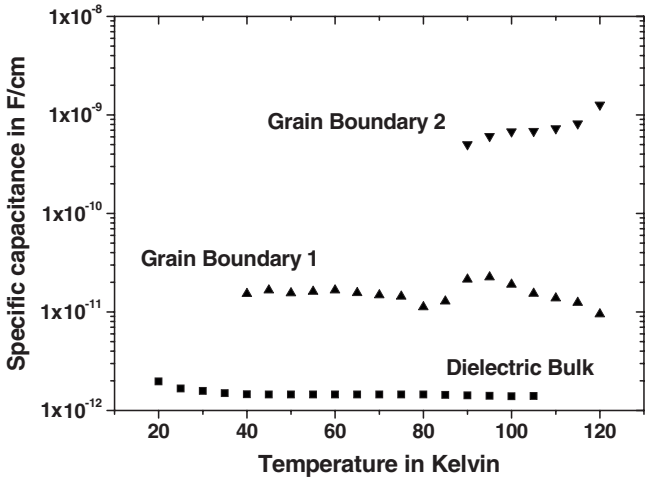

FIG. 7. Specific capacitance for intrinsic bulk, and both GB relaxation processes, plotted vs temperature. Bulk and GB specific capacitance values are in a typical range.

by a factor of ≈10 for the defect and the regular paramagnetic phase. This may be and indication for a relatively high total spin of the magnetic polarons. For comparison, in diluted Sr hole-doped $LaCoO_{3-\delta}$ magnetic polarons were suggested to have spin values of 10–12 (Ref. 5) or 7–10.[31] Taking a value of $S=10$ as a representative estimate of the polaron spin and assuming that the low-temperature magnetic susceptibility data of Fig. 5(a) have a Curie-Weiss-type form, the number of magnetic polarons per f.u. has the approximate value of 0.005. However, this value must be taken as a lower limit since the data of Fig. 5(a) were taken at 10 kOe, and Yamaguchi *et al.*[5] showed that the susceptibility is not field independent at such values of H (for example, see Fig. 4 of Ref. 5). The field and zero-field-cooled magnetization curves in Fig. 5(b) show close agreement, which indicates that the magnetic contributions to the Curie tail may predominantly be paramagnetic.

Inspection of the GB relaxation peak at temperatures near T_{s1} on the z'' vs f scale reveals that the relaxation process splits into two contributions upon heating (Fig. 6); at 80 K the GB relaxation peak becomes slightly asymmetric and two clear peaks are visible at 100 K. This indicates that a second GB-like relaxation process may develop at ≈80 K near the magnetic spin-state transition T_{s1}. At this point it should be stated that it may well be possible that the bulk relaxation peak may split too. However, this could not be investigated because the bulk relaxation peak shifts to frequencies above the resolution limit (1 MHz) at T_{s1}. The appearance of two GB relaxation processes at T_{s1} manifests the coexistence of two electronic phases, which may well be the result of two coexisting magnetic phases. Such correlation would be a typical feature of strongly correlated electron systems, where changes in the net magnetic moment of the electron spins can be reflected in the dielectric structure. The GB relaxation split presented would be consistent with a mixed spin state model, where the two phases above T_{s1} could be associated with the LS and the increasingly populated IS or HS states.

The bulk and both grain-boundary capacitance values are plotted vs T in Fig. 7. The magnitude of the specific capacitance gives a clear indication of the origin of a relaxation.[39] The bulk and both GB capacitance values are all in a very typical range. Therefore, the second GB relaxation process emerging at T_{s1} (GB2) may not be interpreted as an electrode interface effect, where a much larger capacitance would be expected.[39] In order to model data above 80 K, an additional RC element ($R3$-$C3$) was added in series to describe the emerging second GB relaxation (GB2). $R3$ and $C3$ values were determined from Eq. (1b) in Fig. 4 using the f_{max} value of the additional GB relaxation peak (GB2) in the z'' vs f plots at $T>80$ K and from Eq. (3) with $z_0'(f\rightarrow 0)=R1+R2+R3$.

Previously, English *et al.*[33] had observed a distinct change in the dc transport properties at T_{s1} in polycrystalline LCO. The GB resistance observed here is considerably larger than the bulk resistance shown in Fig. 8. Therefore, the appearance of an extra GB relaxation at T_{s1} corresponds well with the observed change in dc resistance in Ref. 33.

The GB and bulk resistivity values plotted in Fig. 8 showed that impurity Mott variable-range hopping (VRH) occurred at $40<T<80$ K with the following ρ vs T dependence:[42,43]

$$\rho = CT^{0.5}\exp\left(\frac{T_0}{T}\right)^{0.25}, \tag{4}$$

where C is a temperature-independent term and T_0 is a characteristic temperature. Deviations from Mott VRH occurred at $T\leq 40$ K, which may be associated with the onset of the magnetic Curie tail (see Fig. 5) and changes in the impurity band structure. At the temperature where the low-temperature GB relaxation splits (into GB1 and GB2), a resistance drop of the first GB relaxation is displayed due to this split. The exact nature of the charge transport for $T\geq 80$ K could not be identified unambiguously, but it may be plausible that the transport properties are influenced by the thermal activation of Co^{3+} electrons from the t_{2g} into the e_g band above T_{s1}.

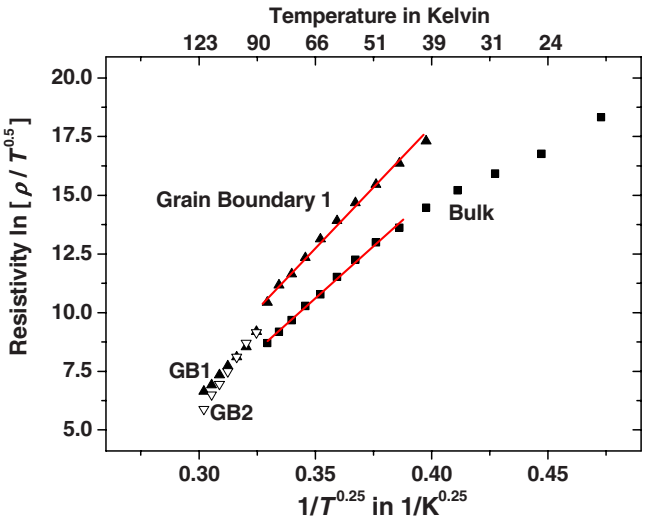

FIG. 8. (Color online) Resistivity ρ for intrinsic bulk, and both GB relaxation processes, plotted vs temperature on Mott variable-range hopping scales $\ln(\rho/T^{0.5})$ vs $1/T^{0.25}$. Red solid lines represent fits to Mott's VRH.

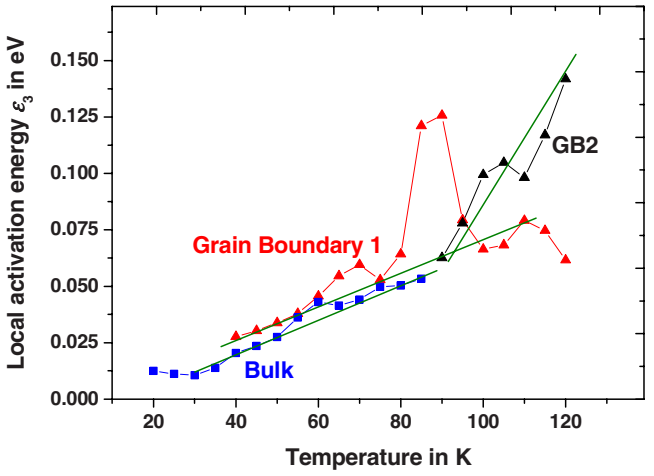

FIG. 9. (Color online) Local activation energy ε_L, in eV, for intrinsic bulk, and both GB relaxation processes plotted vs temperature; ε_L was obtained by differentiating the $\ln(\rho)$ vs $1/T$ curves. Green solid lines are guide to the eyes.

The high GB resistance may be interpreted as a manifestation of GB barrier layers, which limit charge transport. The slopes of the $\ln(\rho/T^{0.5})$ vs $1/T^{0.25}$ curves in the impurity Mott hopping conduction regime at $40<T<80$ K allow the determination of T_0, which is related to the effective density of electron states (DES) N contributing to the impurity charge transport and to the maximum hopping length $r_{\max}$ permitted by the percolation threshold [Eqs. (5a) and (5b)].[43,44] By using an estimated value for the localization length $a=1/\alpha$ of electrons participating to the hopping transport, for example, from the cationic radius of 0.6 Å for Co^{3+} (based on an ionic model neglecting the covalent character of the bonds),[45] the DES near Fermi level $N(\varepsilon_F)$ and $r_{\max}$ at 50 K were calculated according to expressions (5a) and (5b).[43,44] The values are shown in Table I,

$$T_0 = \frac{21.2\alpha^3}{N(\varepsilon_F)k_B}, \tag{5a}$$

$$r_{\max} = 1.073\left(\frac{1}{\alpha N(\varepsilon_F)k_B T}\right)^{1/4}. \tag{5b}$$

The DES values are relatively large and are in a typical range of conventional semiconductors, which is consistent with the low activation energies found in $LaCoO_{3-\delta}$. The relatively short hopping length $r_{\max}$ is also consistent with the high conductivity and semiconducting behavior. The DES values indicate an increase in the density of contributing electron states from the GB to the bulk relaxation. This can be explained by an increase in oxygen vacancy concentration in the bulk as a result of higher oxygen content near the GB areas. Therefore, the GBs show higher resistivity and act as barriers for charge transport. A possible source of error for the DES and $r_{\max}$ calculations may be the underestimate of the Co^{3+} electron localization length a by the ionic radius. A larger a value, i.e., a larger effective electron radius, would result in smaller DES and larger $r_{\max}$ values. The assumption that the covalent character of the bonds may be neglected for the determination of the DES may in fact be doubtful, and the DES and $r_{\max}$ values may represent an estimate only.

The presence of VRH is further demonstrated by the data in Fig. 9, where the gradient of the $\ln(\rho)$ versus $1/T$ curves was interpreted as a local activation energy ε_L for thermally activated charge transport and was plotted versus T in Fig. 9. ε_L values represent the activation energy at one specific temperature only, in contrast to global activation energies E_A.[46] In Fig. 9 it can be seen that local activation energies ε_L are in the range of 0.01–0.06 eV in the bulk, typical of semiconducting behavior. The apparent increase in activation energy with increasing temperature is consistent with VRH. The ε_L values obtained are compatible with previous reports, where an Arrhenius force fit to polycrystalline dc data for $T<80$ K yielded 0.038 eV.

The ε_L values of $\approx$13 meV below 40 K are approximately temperature independent. This deviation from Mott's VRH law was associated with the onset of the magnetic

TABLE I. Characteristic temperature and density of electron states for bulk and GB relaxation processes at $40<T<80$ K.

	T_0 (K)	DES $N(\varepsilon_F)$ near Fermi level $[(\text{eV})^{-1}\ \text{cm}^{-3}]$	Max. hopping length $r_{\max}$ at 50 K(Å)
Bulk	$7.3\times10^7\pm2\times10^6$	$1.56\times10^{22}\pm5\times10^{20}$	10.4
Grain boundary	$1.6\times10^8\pm1\times10^7$	$7.11\times10^{21}\pm4\times10^{20}$	12.7

defect-related Curie tail in the magnetic susceptibility. A crossover from VRH to another thermally activated form of charge transport at very low temperature is unusual and suggests a change in the defect band structure as a consequence of the onset of the defect magnetism.

The peak structure displayed in the main GB activation energy (GB1) corresponds to the resistance drop, where the two GB contributions split, and has therefore no physical meaning. The bulk and GB1 relaxations exhibit a similar increase in charge transport activation energy with temperature as indicated by the solid lines in Fig. 9. The second GB relaxation (GB2) exhibits distinctively different charge transport activation, which may be associated with a transition to a different conduction regime with higher activation energies. It has been reported previously that the activation energy for $T>110$ K in a polycrystal has higher values in the range of 0.15–0.3 eV.[33,47,48]

V. CONCLUSIONS

In conclusion, it can be stated that there is strong evidence for defects dominating resistivity and dielectric properties in polycrystalline $LaCoO_{3-\delta}$ below the spin state transition. The GB relaxation processes exhibit increased resistance and capacitance values compared to the bulk. dc transport measurements carried out previously[33] may be dominated by such GB resistance. The GB dielectric relaxation process splits into two contributions at the magnetic spin state transition T_{s1}, which may be a consequence of magnetic phase coexistence at $T \geq T_{s1}$ of LS and IS/HS states. Dielectric permittivity at $T \leq 40$ K is correlated with the magnetic defect structure. The presence of magnetic point defects at such temperatures also affects the charge transport mechanism in a way that a crossover from impurity Mott's VRH to another type of thermally activated charge transport occurs.

ACKNOWLEDGMENT

The authors wish to thank Neil Hyatt, Derek Sinclair, and Sean Giblin for useful discussions.

*Corresponding author; rainerxschmidt@googlemail.com

[1] M. Imada, A. Fujimori, and Y. Tokura, Rev. Mod. Phys. **70**, 1039 (1998).
[2] K. Asai, P. Gehring, H. Chou, and G. Shirane, Phys. Rev. B **40**, 10982 (1989).
[3] T. Vogt, J. A. Hriljac, N. C. Hyatt, and P. Woodward, Phys. Rev. B **67**, 140401(R) (2003).
[4] J. C. Burley, J. F. Mitchell, and S. Short, Phys. Rev. B **69**, 054401 (2004).
[5] S. Yamaguchi, Y. Okimoto, H. Taniguchi, and Y. Tokura, Phys. Rev. B **53**, R2926 (1996).
[6] G. Maris, Y. Ren, V. Volotchaev, C. Zobel, T. Lorenz, and T. T. M. Palstra, Phys. Rev. B **67**, 224423 (2003).
[7] M. A. Señarís-Rodríguez and J. B. Goodenough, J. Solid State Chem. **116**, 224 (1995).
[8] M. A. Korotin, S. Y. Ezhov, I. V. Solovyev, V. I. Anisimov, D. I. Khomskii, and G. A. Sawatzky, Phys. Rev. B **54**, 5309 (1996).
[9] D. Louca and J. L. Sarrao, Phys. Rev. Lett. **91**, 155501 (2003).
[10] A. Ishikawa, J. Nohara, and S. Sugai, Phys. Rev. Lett. **93**, 136401 (2004).
[11] R. R. Heikes, R. C. Miller, and R. Mazelsky, Physica **30**, 1600 (1964).
[12] G. H. Jonker, J. Appl. Phys. **37**, 1424 (1966).
[13] P. M. Raccah and J. B. Goodenough, Phys. Rev. **155**, 932 (1967).
[14] M. W. Haverkort *et al.*, Phys. Rev. Lett. **97**, 176405 (2006).
[15] A. Podlesnyak, S. Streule, J. Mesot, M. Medarde, E. Pomjakushina, K. Conder, A. Tanaka, M. W. Haverkort, and D. I. Khomskii, Phys. Rev. Lett. **97**, 247208 (2006).
[16] C. Zobel, M. Kriener, D. Bruns, J. Baier, M. Grüninger, T. Lorenz, P. Reutler, and A. Revcolevschi, Phys. Rev. B **66**, 020402(R) (2002).
[17] T. Kyômen, Y. Asaka, and M. Itoh, Phys. Rev. B **67**, 144424 (2003).
[18] K. Asai, A. Yoneda, O. Yokokura, J. M. Tranquada, G. Shirane, and K. Kohn, J. Phys. Soc. Jpn. **67**, 290 (1998).
[19] S. Stølen, F. Grønvold, H. Brinks, T. Atake, and H. Mori, Phys. Rev. B **55**, 14103 (1997).
[20] K. Asai, O. Yokokura, N. Nishimori, H. Chou, J. M. Tranquada, G. Shirane, S. Higuchi, Y. Okajima, and K. Kohn, Phys. Rev. B **50**, 3025 (1994).
[21] M. Tachibana, T. Yoshida, H. Kawaji, T. Atake, and E. Takayama-Muromachi, Phys. Rev. B **77**, 094402 (2008).
[22] J. B. Goodenough, J. Alloys Compd. **262-263**, 1 (1997).
[23] K. Knižek, Z. Jirák, J. Hejtmánek, P. Henry, and G. André, J. Appl. Phys. **103**, 07B703 (2008).
[24] D. P. Kozlenko, N. O. Golosova, Z. Jirak, L. S. Dubrovinsky, B. N. Savenko, M. G. Tucker, Y. Le Godec, and V. P. Glazkov, Phys. Rev. B **75**, 064422 (2007).
[25] S. Yamaguchi, Y. Okimoto, and Y. Tokura, Phys. Rev. B **55**, R8666 (1997).
[26] P. G. Radaelli and S. W. Cheong, Phys. Rev. B **66**, 094408 (2002).
[27] E. L. Nagaev and A. I. Podelshchikov, J. Phys.: Condens. Matter **8**, 5611 (1996).
[28] S. R. Giblin, I. Terry, S. J. Clark, T. Prokscha, D. Prabhakaran, A. T. Boothroyd, J. Wu, and C. Leighton, Europhys. Lett. **70**, 677 (2005).
[29] A. Podlesnyak *et al.*, Phys. Rev. Lett. **101**, 247603 (2008).
[30] D. Phelan *et al.*, Phys. Rev. Lett. **96**, 027201 (2006).
[31] Z. Jirak, J. Hejtmanek, K. Knizek, and M. Veverka, Phys. Rev. B **78**, 014432 (2008).
[32] Y. Tokura, Y. Okimoto, S. Yamaguchi, H. Taniguchi, T. Kimura, and H. Takagi, Phys. Rev. B **58**, R1699 (1998).
[33] S. R. English, J. Wu, and C. Leighton, Phys. Rev. B **65**, 220407(R) (2002).
[34] W. Eerenstein, N. D. Mathur, and J. F. Scott, Nature (London) **442**, 759 (2006).

[35] T. Kimura, T. Goto, H. Shintani, K. Ishizaka, T. Arima, and Y. Tokura, Nature (London) **426**, 55 (2003).
[36] J. Wu and C. Leighton, Phys. Rev. B **67**, 174408 (2003).
[37] R. Schmidt, in *Ceramic Materials Research Trends*, edited by P. B. Lin (Novascience, Hauppauge, 2007), p. 321.
[38] *Impedance Spectroscopy*, edited by J.R. Macdonald (Wiley, New York, 1987).
[39] J. T. S. Irvine, D. C. Sinclair, and A. R. West, Adv. Mater. (Weinheim, Ger.) **2**, 132 (1990).
[40] R. Schmidt and A. W. Brinkman, Adv. Funct. Mater. **17**, 3170 (2007).
[41] I. Terry, S. von Molnar, A. M. Torressen, and P. Becla, Philos. Mag. B **65**, 1245 (1992).
[42] N. F. Mott, *Conduction in Non-Crystalline Materials* (Clarendon Press, Oxford, 1993).
[43] B. I. Shklovskii and A. L. Efros, *Electronic Properties of Doped Semiconductors* (Springer-Verlag, Berlin, 1984).
[44] R. Schmidt, A. Basu, and A. W. Brinkman, Phys. Rev. B **72**, 115101 (2005).
[45] R. D. Shannon, Acta Crystallogr., Sect. A: Cryst. Phys., Diffr., Theor. Gen. Crystallogr. **32**, 751 (1976).
[46] R. Schmidt, Phys. Rev. B **77**, 205101 (2008).
[47] M. A. Señarís-Rodríguez and J. B. Goodenough, J. Solid State Chem. **118**, 323 (1995).
[48] E. Iguchi, K. Ueda, and W. H. Jung, Phys. Rev. B **54**, 17431 (1996).